Hindawi
Geofluids
Volume 2023, Article ID 1743305, 10 pages
https://doi.org/10.1155/2023/1743305

Research Article

Propagation Mechanism of Deep-Water Impulse Waves Generated by Landslides in V-Shaped River Channels of Mountain Valleys: Physical Model of Regular Rigid Block

Rubin Wang,[1,2] **Yunzi Wang**,[1] **Jianxin Wan**,[2] **Weiya Xu**,[1] **Yue Yang**,[2] **and Huanling Wang**[1]

[1]*Key Laboratory of Ministry of Education for Geomechanics and Embankment Engineering, Hohai University, Nanjing, China*
[2]*Research Institute of Geotechnical Engineering, Hohai University, Nanjing, China 210098*

Correspondence should be addressed to Rubin Wang; rbwang@hhu.edu.cn

Received 30 September 2022; Revised 1 November 2022; Accepted 24 November 2022; Published 8 February 2023

Academic Editor: Yiding Bao

Landslide-induced impulse waves in alpine valleys are a significant risk to large-scale dam and reservoir engineering projects in the surrounding area. In this study, a 1 : 200-scale physical model of landslide-induced impulse waves in a V-shaped river channel was established, and 18 groups of tests were conducted to evaluate the influence of different parameters, such as the volume and shape of the landslide body, water entry velocity, and water depth of the reservoir. Based on the test results, a dimensionless formula was established for the first wave height of impulse waves caused by a deep-water landslide in a V-shaped channel. An energy conversion law was determined for the impact of landslide-induced impulse waves on the reservoir bank. Finally, a distribution law was obtained for the initial maximum pressure caused by landslide-induced impulse waves along the water depth on the opposite bank. The theoretical predictions of the dimensionless formula showed good agreement with the experimental results, and the energy conversion rate of the landslide-induced impulse waves initially increased and then decreased with an increasing Froude number. The maximum dynamic water pressure showed a triangular distribution with increasing water depth below the surface of the still water body. The impact pressure of the impulse waves on the slope on the opposite bank increased with the water entry velocity. This study provides a scientific basis for the risk prevention and control of landslide-induced impulse waves in river channels feeding into reservoirs.

1. Introduction

High-velocity landslides in alpine areas and gorges produce huge impulse waves that feature short generation and propagation times, fast velocities, and a wide disaster range. Around major hydropower projects, they can not only wash away hydraulic structures and block river channels but may also cause serious accidents such as dam failure. In 1963, a landslide at Vajont Dam in Italy caused a huge wave with a height of up to 175 m, which destroyed a 70 m high concrete dam, washed away the town of Longaroni and five nearby villages, and claimed nearly 2000 lives. In 1985, a landslide in Xintan, Zigui, near China's Three Gorges Dam, induced impulse waves that climbed up to a height of 54 m. The impulse waves overturned four fishing boats 2 km upstream and spread 42 km upstream and downstream to cause more than ten deaths. Therefore, research on landslide-induced impulse waves in alpine areas can provide a crucial reference for early warning and risk prevention of disasters in high dams and large reservoirs.

Various methods have been used in the research and analysis of landslide-induced impulse waves, e.g., analytical solutions [1–4], numerical simulations [5–8], physical models [9–14], and field data analysis [15, 16]. Because the location and time that a landslide enters the water cannot be accurately predicted in advance, obtaining original data on landslide-induced impulse waves is difficult. Thus, physical models are used to simulate landslide-induced impulse

waves and obtain characteristic parameters such as the first wave height, propagation process, and impact pressure. This approach is widely used to research landslide-induced impulse waves in alpine areas.

Previous models of landslide-induced impulse waves have considered the influence of the water entry velocity, volume, angle, and density of the landslide body. However, these models mostly used rectangular or trapezoidal channels to represent rivers. Few studies have considered the propagation process and impact pressure distribution of landslide-induced impulse waves in V-shaped river channels, which are common in alpine areas. The slopes of the banks on both sides of a V-shaped channel significantly affect the formation and propagation of landslide-induced impulse waves. Compared with rivers in plains and flat lands, impulse waves in V-shaped river channels in alpine areas have a more obvious disaster chain. The narrow river channel means that the landslide body can easily block it upon entry, which would greatly increase the overall water depth and may even form a dam that threatens the downstream area. In addition, the opposite bank confines the huge kinetic energy generated by the landslide-induced impulse waves and does not let it dissipate. This increases the impact pressure on the banks and dam bodies, which affects the stability and safety of the facilities. Even worse, the impulse waves may strike the opposite bank directly, which would damage infrastructure along the riverfront and threaten the safety of people and property.

In this study, a 1 : 200-scale physical model was established to reveal the characteristics of deep-water landslide-induced waves in V-shaped river channels. Experiments were performed to consider the influence of the volume, shape, and velocity of the landslide body and the water depth of the reservoir. A dimensionless formula was derived for the first wave height in the V-shaped channel. An energy conversion law was obtained for the impulse waves, and a distribution law was obtained for the initial maximum dynamic water pressure on the opposite bank along the water depth. This study provides a scientific reference for the risk prevention and control of landslide-induced impulse waves in the alpine areas of major hydropower projects.

2. Materials and Methods

A 1 : 200-scale physical model was established based on the gravity similarity criterion and Froude similarity criterion, as shown in Figure 1. A high-definition camera was installed on one side of the tank to capture the landslide body as it slid into the water and the resulting impulse waves. Wave height gauges N.1, N.2, and N.3 were set in the channel at a spacing of 1.2 m. Wave height gauge N.4 was installed on the opposite bank to record the rise of impulse waves. The wave height gauges measured the wave height at a frequency of 50 Hz and a resolution of 0.1 mm. Eight water pressure sensors (P1–P8) were arranged on the opposite bank to measure the impact pressure of the impulse waves at a collection frequency of 50 Hz and resolution of 0.01 kPa. The pressure sensor P1, which was 73 cm away from the bottom of the river channel, was arranged at the central axis of the opposite bank. The positions of other sensors are shown in Figure 1.

In the experimental model, the inclination of the sliding bed was 34°, the inclination of the opposite bank was 43°, and the fall height of the center of mass of the block was 1.8 m. The water depth of the V-shaped channel was between 0.86 and 1.26 m. According to the geotechnical characteristic of landslides, they are divided into two types: loose earth landslides and rock landslides. This experiment studied rock landslides [17–19]. As shown in Figure 2, the landslide body was represented by concrete blocks of different shapes that had a density of 2300 kg/m^3, length of 0.45–0.55 m, width of 0.3–0.4 m, and thickness of 0.1–0.27 m. The width of the experimental slot was 0.66 m. All landslide bodies were narrower than the width of the slot, and the generated impulse waves propagated in the lateral direction. The velocity of the landslide body was controlled by a sliding control device. The sliding velocity was measured by a Hall velocity sensor connected to the landslide body at a resolution of 0.01 m/s.

An orthogonal design was adopted for the experiments with the physical model. The maximum wave amplitude, which corresponded to the maximum water entry velocity, was assumed to be the first wave amplitude. After the landslide-induced impulse waves propagated, the distance between the first two crests was measured and was taken as the wavelength. Table 1 presents the experimental design and results. The test parameters included the length (l), width (w), and thickness (s) of the landslide body, as well as the still water depth (h_0), sliding bed inclination angle (α), and water entry velocity of the landslide body (u). The results were represented by the Froude number (F), first wave amplitude (a), and wave celebrity (c).

3. Results and Discussion

3.1. Generation and Propagation Characteristics. The velocity at which a landslide body enters the water is an important factor that affects the generation and propagation of impulse waves. However, the difficulty of measuring the water entry velocity has limited the number of related studies. Fritz et al. [10] and Heller et al. [20] used particle image velocimetry and a laser distance sensor to track and measure the vector field for the near-field impulse wave velocity. To analyze the impact velocity of the landslide, they used the calculation formula presented by Körner [21].

$$u = \sqrt{2g\Delta z(1 - f\cot\alpha)}, \tag{1}$$

where u is the water entry velocity of the center of mass of the landslide body (m/s), g is the acceleration of gravity (m/s^2), Δz is the height between the original center of the mass and the static water depth (m), f is the friction coefficient, and α is the inclination angle of the sliding bed (°). Equation (1) ignores the effects of air resistance, underwater friction, and water resistance, so the water entry velocity u increases with an increase in any of the other terms.

The sliding velocity control device was used to increase the sliding velocity of the landslide body before entering

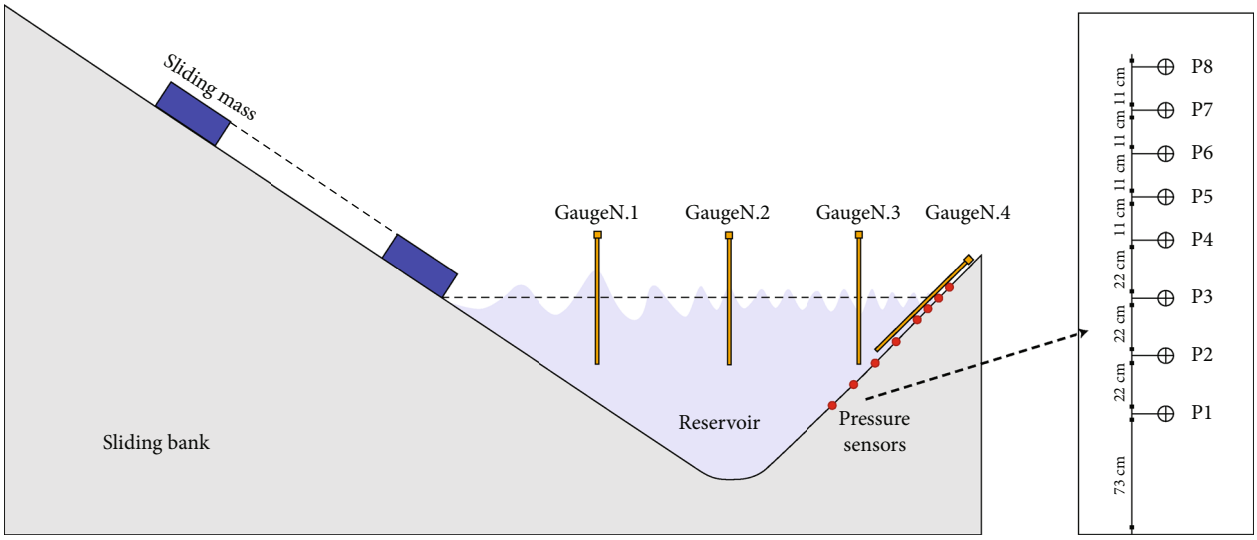

Figure 1: Schematic diagram of the physical model.

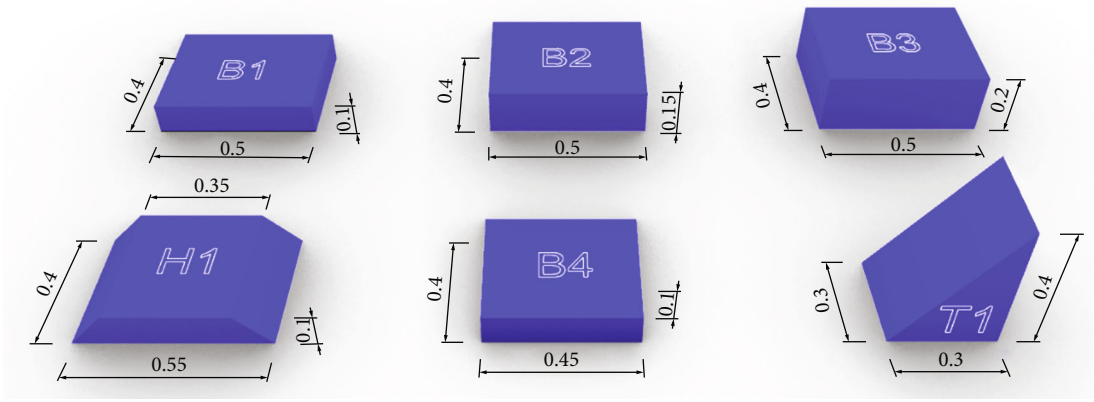

Figure 2: Schematic diagram of regular rigid blocks representing the landslide body (dimensions: m).

the water to 0.67, 1.16, and 1.67 m/s. The changes in the sliding velocity and acceleration as the landslide body entered the water were obtained. As shown in Figure 3, the landslide body initially showed an approximately linear increase in velocity followed by a slow acceleration or deceleration and a rapid deceleration to a final stop. These three stages corresponded to the landslide body sliding in air, sliding in water, and bottoming out, respectively. The duration of the second stage (i.e., slow acceleration or deceleration) differed with the water depth.

Figure 4 shows the three stages of the sliding acceleration for each sliding velocity. Because the sliding bed and landslide body were controlled by a mechanical transmission device, the initial velocity of the landslide body was provided by the control device. Before the landslide body reached the still water surface, the reduction in acceleration was mainly caused by the friction between the sliding bed surface and the landslide body. After the block entered the water, the acceleration was affected by the friction from the sliding bed surface and the viscous resistance of the water, so it became negative. The resistance reached its maximum when the front end of the landslide body reached the bottom of the river, which caused the landslide body to quickly decelerate and stop.

Based on the results of the physical model, the generation and propagation of landslide-induced impulse waves in a V-shaped river channel can be summarized into three stages. In the first stage, the landslide body entered the water body quickly; the front edge of the landslide body hit and displaced part of the water body. A small part of the displaced water body jumped from the water surface to form a water tongue, and most of the water body near the water entry point was compressed and increased in height, which formed the first wave. In the second stage, the landslide body slid into the water body and transferred energy continuously. It displaced more of the water body, which caused the leading edge of the rising wave to move forward, while the trailing edge moved toward the impact crater that was generated by the landslide body when it struck the water body because of gravity. The water tongue formed by the impact then began to splash back into the water. In the third stage, the landslide body stopped moving and completed the process of transferring energy to the water. Then, water converted the kinetic energy to form impulse waves that spread to the opposite bank.

Table 1: Experimental design and test results.

No.	Landslide body	Test parameters							Test results	
		l (m)	w (m)	s (m)	h_0 (m)	α (°)	u (m/s)	F	a (m)	c (m/s)
1	B1	0.50	0.40	0.10	0.86	34	1.16	0.40	0.037	2.89
2	B1	0.50	0.40	0.10	1.10	34	1.67	0.51	0.064	3.33
3	B1	0.50	0.40	0.10	1.26	34	0.67	0.19	0.014	2.95
4	B2	0.50	0.40	0.15	0.86	34	1.67	0.58	0.098	3.42
5	B2	0.50	0.40	0.15	1.10	34	0.67	0.20	0.026	3.03
6	B2	0.50	0.40	0.15	1.26	34	1.16	0.33	0.059	2.97
7	B3	0.50	0.40	0.20	0.86	34	0.67	0.23	0.052	2.77
8	B3	0.50	0.40	0.20	1.10	34	1.16	0.35	0.088	2.94
9	B3	0.50	0.40	0.20	1.26	34	1.67	0.47	0.107	3.23
10	B4	0.45	0.40	0.10	0.86	34	0.67	0.23	0.028	2.60
11	B4	0.45	0.40	0.10	1.10	34	1.16	0.35	0.036	3.10
12	B4	0.45	0.30	0.10	1.26	34	1.67	0.48	0.070	3.42
13	T1	0.50	0.30	0.27	0.86	34	1.67	0.58	0.111	3.57
14	T1	0.50	0.30	0.27	1.10	34	0.67	0.20	0.030	3.10
15	T1	0.50	0.30	0.27	1.26	34	1.16	0.33	0.061	3.33
16	H1	0.55	0.40	0.10	0.86	34	1.16	0.40	0.048	3.20
17	H1	0.55	0.40	0.10	1.10	34	1.67	0.51	0.075	3.42
18	H1	0.55	0.40	0.10	1.26	34	0.67	0.18	0.017	3.09

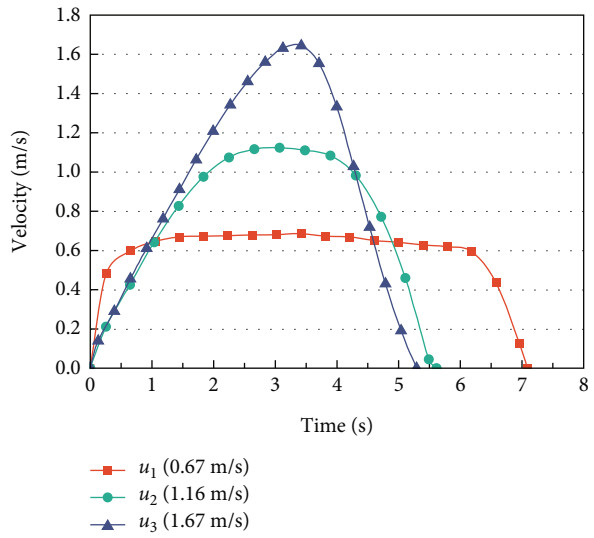

Figure 3: Changes in velocity before and after the landslide body entered the water at three sliding velocities.

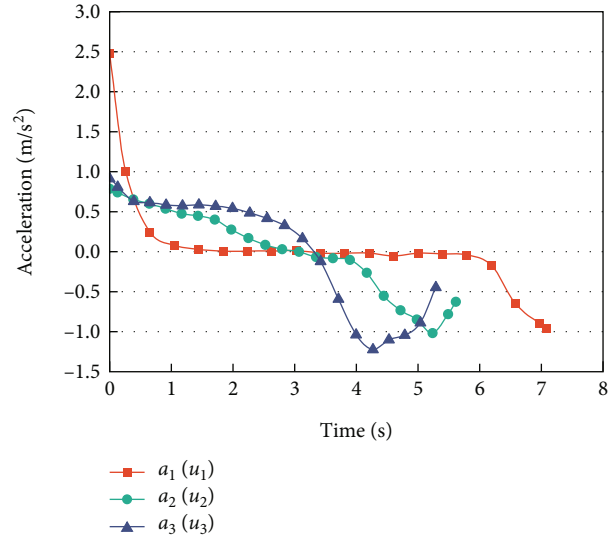

Figure 4: Changes in acceleration before and after the landslide body entered the water at three sliding velocities.

To reveal the influence of the shape and water entry velocity of the landslide body on the propagation of impulse waves, the monitoring data of key wave height gauges were selected, and 18 groups of time history curves for the amplitudes of the landslide-induced impulse waves were obtained, as shown in Figure 5. The impulse waves featured the formation of an advancing wave train dominated by waves with positive amplitudes (i.e., wave crests). The first or second wave crests had the largest amplitude, followed by oscillating waves of smaller amplitude. The largest trough occurred before the highest crest. In general, the different shapes of the landslide bodies generated similar impulse waves on the opposite bank, but the amplitude and period differed.

3.2. Waveform Characteristics. According to the experimental results of Noda [3] and Fritz et al. [1], the waveforms of landslide-induced impulse waves in the near-field region can be divided into weakly nonlinear oscillatory waves ($F < 4 - 7.5S$), nonlinear transition waves ($4 - 7.5S \le F < 6.6 - 8S$), solitary waves ($6.6 - 8S \le F < 8.2 - 8S$), and dissipative transient bores ($F \ge 8.2 - 8S$). Each waveform, which was dependent on the Froude number ($F = u/\sqrt{gh_0}$) of

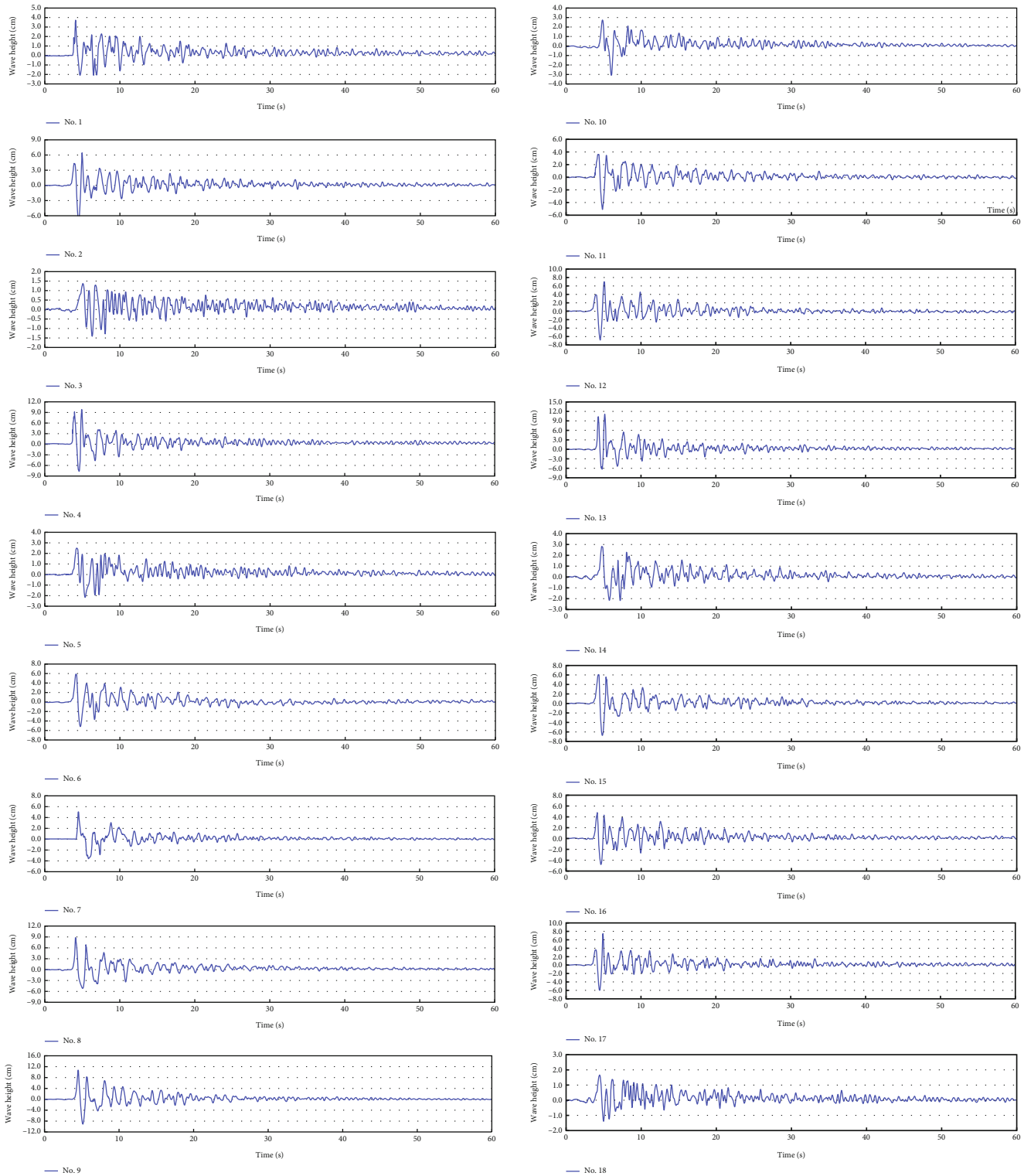

Figure 5: Time history curves of 18 groups of wave amplitudes measured by wave height gauge no. 1.

the landslide body, struck the water body and the relative thickness of the landslide body ($S = s/h_0$). F was less than ($4 - 7.5S$) in all 18 groups of tests, so the impulse waves were all weakly nonlinear oscillatory waves.

The wave amplitude and velocity are important characteristics of landslide-induced impulse waves. Previous studies have shown that the geometric size of the landslide body, water depth, and water entry velocity are the controlling factors of the first wave amplitude. In this study, nonlinear regression analysis was used to identify the correlation between the geometric dimensions of the landslide body, water depth in front of the slope, and water entry velocity

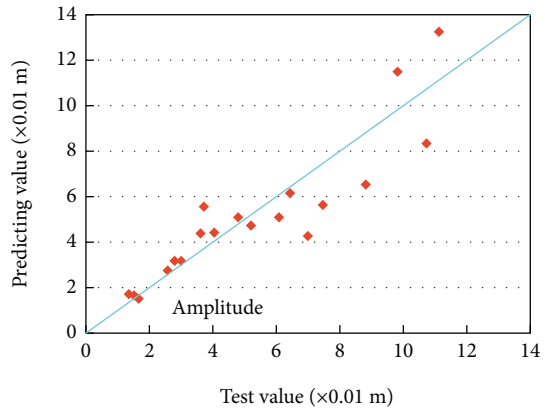

Figure 6: Predicted and experimental values of the first wave amplitude.

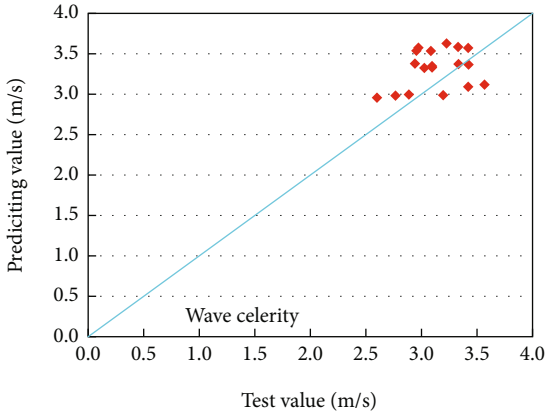

Figure 7: Calculated and experimental values of the wave celerity.

of the landslide body. A dimensionless formula was obtained for the first wave amplitude in a V-shaped river channel:

$$\frac{a}{h_0} = 0.951\left(\frac{u}{\sqrt{gh_0}}\right)^{1.197}\left(\frac{l}{h_0}\right)^{-1.013}\left(\frac{w}{h_0}\right)^{0.990}\left(\frac{s}{h_0}\right)^{0.717}, \quad (2)$$

where $(u/\sqrt{gh_0})$ is the relative water entry velocity, (l/h_0) is the relative length, (w/h_0) is the relative width, and (s/h_0) is the relative thickness of the landslide body. Figure 6 compares the predicted first wave amplitude via Equation (2) with the test results. A correlation coefficient of 0.82 was obtained.

The wave velocity describes the propagation distance of a waveform per unit time, and it is an important parameter for calculating the propagation of landslide-induced impulse waves. The following empirical formula for nonlinear waves is usually used for prediction.

$$c = \sqrt{g(h_0 + a)}. \quad (3)$$

Figure 7 compares the prediction results of Equation (3) with the measured test data. The correlation coefficient was 0.551, with a maximum error of 16.8% and an average error

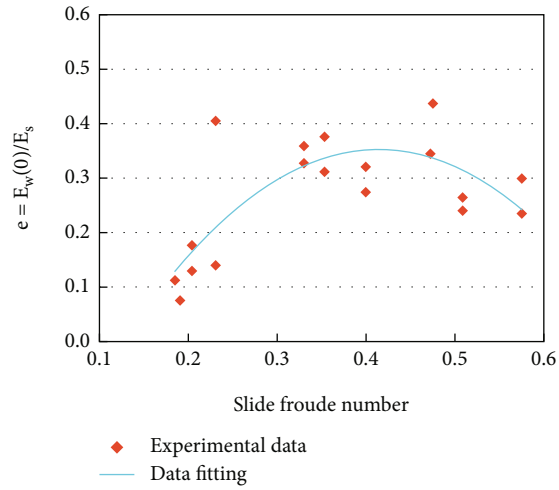

Figure 8: Energy conversion rate at different Froude numbers.

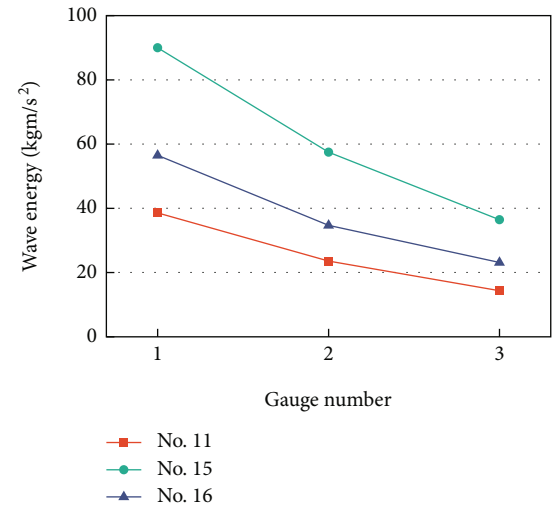

Figure 9: Wave energy of different shapes for the landslide body measured by different wave height gauges.

of 9.1%. The error can be attributed to the frame rate of the camera. Although the correlation was low, it was numerically close. Therefore, the theoretical formula of wave celerity can be used to predict the celerity of the impulse wave [22].

Dimensionless functions are commonly used in regression analysis for prediction. Similar to Equation (2), a series of dimensionless power exponents are multiplied, which are usually specific values of the same controlling factor. Different scholars have used different controlling factors for regression analysis. Noda [3] proposed the method of calculating the maximum impulse wave height based on a linear relationship with the Froude number. Fritz et al. [1] proposed the method of calculating the maximum impulse wave height based on the Froude number and relative thickness. Ataie-Ashtiani and Nik-khah [9] proposed the method of calculating the maximum impulse wave height by considering factors such as the dimensionless sliding volume, Froude number, inclination angle of the sliding surface, and underwater sliding time. Zweifel et al. [23] proposed another method of calculating the maximum impulse wave height

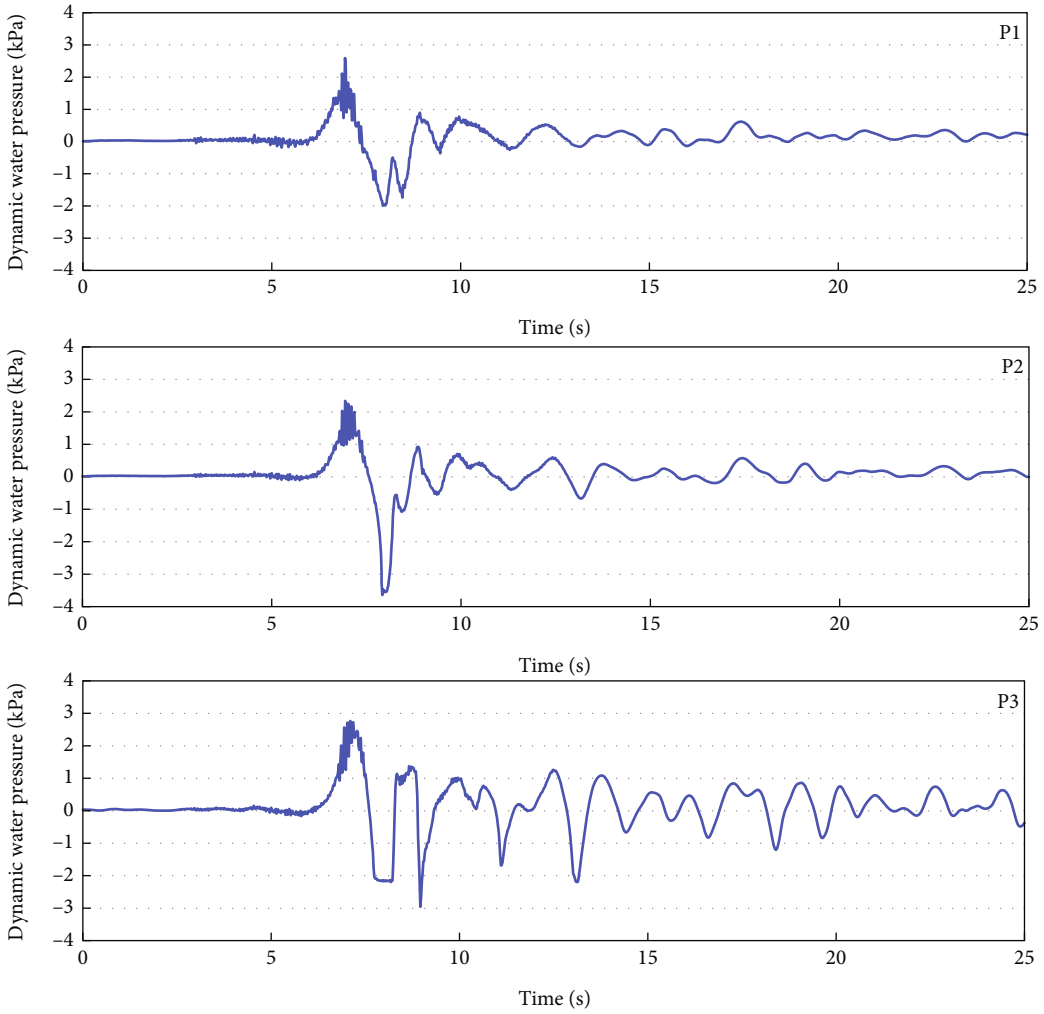

Figure 10: Time history curves of the dynamic water pressure with landslide body T1 at measurement points P1–P3.

by considering the Froude number, relative thickness, and relative mass. The power exponents of each variable in the equations proposed by the above researchers varied substantially; in particular, the power exponent of the Froude number was between 0.2 and 1.4. A larger power exponent for the Froude number indicated a greater influence of the relative velocity on the wave height and vice versa. For V-shaped channels, the wave height of landslide-induced impulse waves increased significantly with the water entry velocity of the landslide body. The dimensionless formula proposed for the first wave amplitude of the V-shaped channel (i.e., Equation (2)) confirmed this cognition, which reflected its applicability and rationality.

3.3. Energy Characteristics. The main characteristics of landslide-induced impulse waves are closely related to the law of energy transfer of the landslide mass. The time history curves of the wave heights collected by the wave height gauges were used to calculate the wave energy as follows according to Ataie-Ashtiani and Nik-khah [9]:

$$E_w = 2E_{\text{pot}} = \rho_w g c \int \eta^2 dt, \tag{4}$$

where E_w is the wave energy per unit width (kg m/s^2), E_{pot} is the wave potential energy per unit width (kg m/s^2), ρ_w is the density of water (1000 kg/m^3), g is the acceleration of gravity (9.8 m/s^2), c is the wave velocity (m/s), η is the water surface elevation when the water body is still (m), and t is the time (s).

The energy of the landslide body can be calculated by using the Watts [24] formula:

$$E_s = \rho_s u^2 A, \tag{5}$$

where E_s is the energy of the landslide body per unit width (kg m/s^2), ρ_s is the density of the landslide body (kg/m^3), u is the water entry velocity of the landslide body (m/s), and A is the cross-sectional area of the landslide body (m^2). The wave energy conversion rate of the impulse waves is expressed by [25]

$$e_0 = \frac{E_w(0)}{E_s}, \tag{6}$$

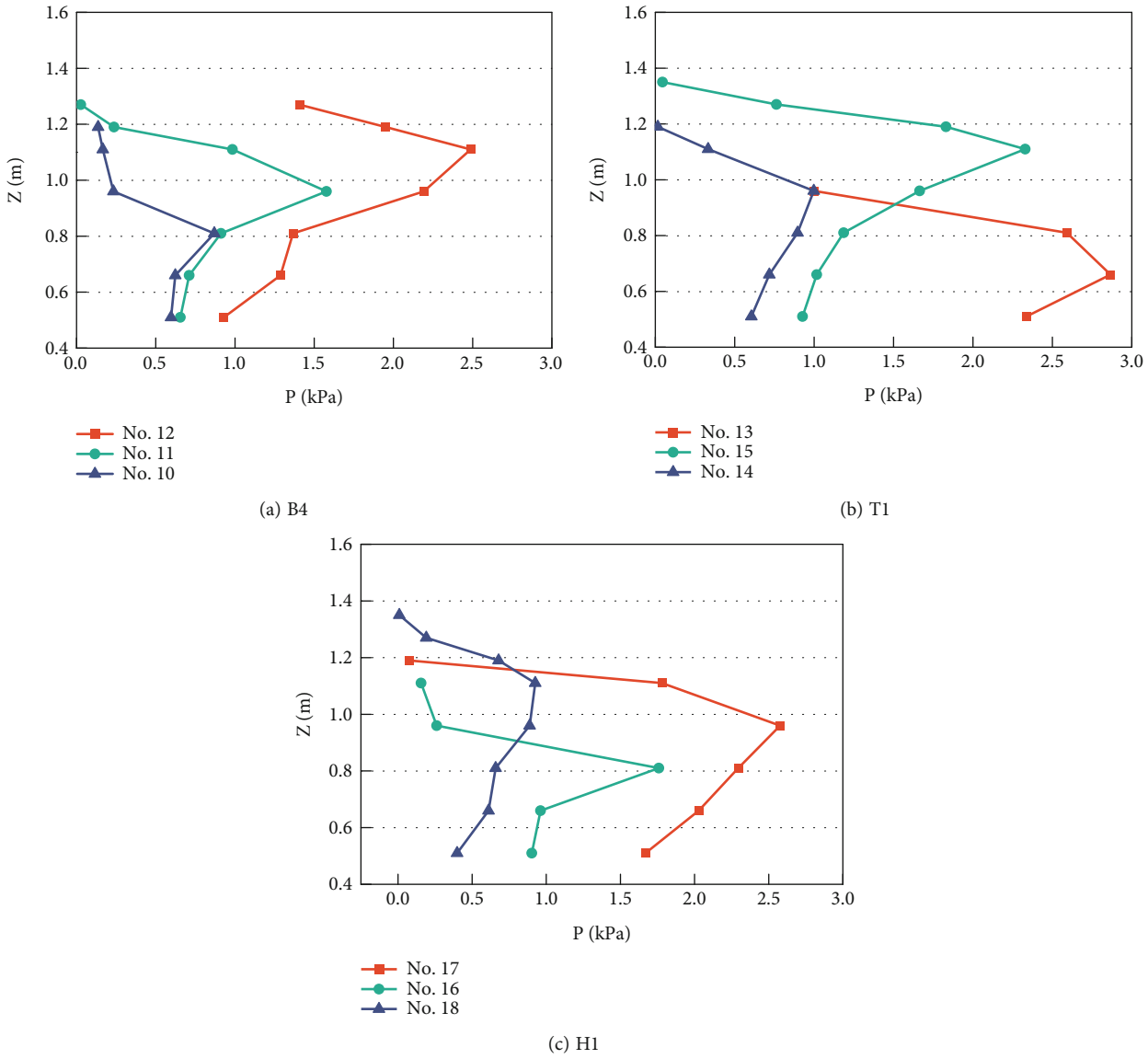

Figure 11: Impact pressure distributions from the impulse waves of landslide bodies B4, T1, and H1 on the opposite bank (Nos. 10–18).

where $E_w(0)$ is the wave energy in the near-field area of impulse wave generation. Figure 8 shows the changes in the energy conversion rate of the landslide-induced impulse waves at different Froude numbers according to the measurements of the wave height gauges. The energy conversion rate initially increased and then decreased as the Froude number F increased.

Figure 9 shows the changes in the wave energy according to the position of the wave height gauges for landslide bodies with different shapes. Tests 11, 15, and 16 all had the same water entry velocity and corresponded to landslide bodies with the shapes of B4, T1, and H1, respectively. T1 had the greatest wave energy, followed by H1 and then B4. Similarly, T2 showed the greatest propagation decay in the wave energy, followed by H1 and then B4. Therefore, landslide bodies with different shapes followed a similar law of energy propagation; however, the attenuation of the wave energy during the propagation process differed.

3.4. Impact Pressure Characteristics. The formation and propagation of landslide-induced waves in V-shaped river channels in alpine valleys are significantly affected by the slopes of the banks on both sides. The slope on the opposite bank constrains the huge kinetic energy generated by the impulse waves induced by the entry of the landslide body, so it cannot dissipate in time. This produces higher impulse waves that propagate to the opposite bank, which poses a huge threat to the safety of the local infrastructure and residents. Studying the impact pressure of landslide-induced waves on the banks of river channels is of great significance for preventing and controlling disasters.

In the physical model, eight pressure sensors were installed on the opposite bank. Impulse waves propagated to the opposite bank, and the impact pressure was measured by the sensors. Figure 10 shows the time history curve of the hydrodynamic pressure measured by sensors P1–P3 in test 13, which used landslide body T1. The waves reflected,

superimposed, and oscillated after they propagated to the opposite bank. The hydrodynamic pressure curves had the same wave amplitude, and the maximum value was affected by the water depth of the channel and the water entry velocity of the landslide body.

The influence of the shape of the landslide body, the water depth of the river channel, and the water entry velocity of the landslide body on the impact pressure distribution were investigated: three typical shapes of landslide bodies were selected—B4, T1, and H1. The water depth was set to 0.86, 1.10, and 1.26 m. The water entry velocity was set to 0.67, 1.16, and 1.67 m/s. Figure 11 shows the impact pressure distributions generated by landslide-induced waves. The impact pressure distributions generated by different shapes of landslide bodies generally had the same pattern. The main difference among the landslide bodies was in the frontal area that entered the water. For a given water entry velocity, a larger frontal area increased the impact pressure. The increase in the water entry velocity reduced the time for the landslide body to reach the bottom, which increased the amplitude of the waves that caused the impact pressure. At different water depths, the distributions of the maximum impact pressure on the opposite bank and the maximum amplitude of the impulse waves were generally the same. However, with the increasing water depth, the impact pressure distribution fluctuated at lower depths, indicating the complexity of the energy transfer when a landslide struck deep water.

The results indicate that the maximum dynamic water pressure is caused by the initial wave and that it follows an approximately triangular distribution along the water depth. The potential energy of the landslide body is instantaneously converted into kinetic energy after it enters the water, which applies a huge impact pressure on the water body. This pressure acts on the water body along the entire depth and generates impulse waves at the surface of the water body. The impulse waves propagate to the opposite bank as the potential energy is converted to kinetic energy. Because of the narrow dimensions of the V-shaped channel, the energy cannot dissipate in time, which increases the pressure transmitted to the opposite bank.

4. Conclusion

A physical model was used to perform 18 tests under different conditions to characterize the propagation of landslide-induced waves and the impact pressure distribution in V-shaped river channels in alpine valleys that contain major hydropower projects. The main conclusions are as follows:

(1) The impulse waveforms were all weakly nonlinear oscillatory waves. The waves generally formed an advancing wave train with positive amplitudes (wave crest) followed by oscillating waves with smaller amplitudes

(2) The results of the nonlinear regression analysis were used to propose a dimensionless equation for the amplitude of the first wave induced by a landslide in a V-shaped river channel. The prediction results obtained using the proposed equation showed a strong correlation with the observed results of the physical model at a correlation coefficient of 0.82

(3) An energy transformation law was obtained for landslide-induced impulse waves in a V-shaped river channel. The wave energy conversion rate initially increases and then decreases with an increasing Froude number. The shape of the landslide body does not significantly affect the energy propagation law but significantly affects the degree of wave energy attenuation

(4) The distribution of the maximum dynamic water pressure caused by landslide-induced waves in a V-shaped river channel on the opposite bank was obtained. The distribution is approximately triangular along the water depth; the pressure reaches a maximum value near the surface of the still water body and gradually decreases from the surface downward

Data Availability

An orthogonal design was adopted for the experiments with the physical model. The maximum wave amplitude, which corresponded to the maximum water entry velocity, was assumed to be the first wave amplitude. After the landslide-induced impulse waves propagated, the distance between the first two crests was measured and was taken as the wavelength. Table 1 presents the experimental design and results. The test parameters included the length (l), width (w), and thickness (s) of the landslide body, as well as the still water depth (h_0), sliding bed inclination angle (α), and water entry velocity of the landslide body (u). The results were represented by the Froude number (F), first wave amplitude (a), and wave velocity (c).

Conflicts of Interest

The authors declare no competing interests.

Acknowledgments

This work is supported by the National Natural Science Foundation of China (No. 51939004) and the Fundamental Research Funds for the Central Universities (No. B200204008). We are also deeply indebted and grateful and owe our thanks to the Guiyang Engineering Corporation Limited of PowerChina for assistance in the collection of engineering geological exploration data.

References

[1] H. M. Fritz, W. H. Hager, and H. E. Minor, "Landslide generated impulse waves," *Experiments in Fluids*, vol. 35, no. 6, pp. 505–519, 2003.

[2] S. T. Grilli and P. Watts, "Tsunami generation by submarine mass failure. I: modeling, experimental validation, and sensitivity analyses," *Journal of Waterway Port Coastal & Ocean Engineering*, vol. 131, no. 6, pp. 283–297, 2005.

[3] E. Noda, "Water waves generated by landslides," *Journal of the Waterways Harbors & Coastal Engineering Division*, vol. 96, no. 4, pp. 835–855, 1970.

[4] S. A. Rzadkiewicz, C. Mariotti, and P. Heinrich, "Modelling of submarine landslides and generated water waves," *Physics & Chemistry of the Earth*, vol. 21, no. 1, pp. 7–12, 1996.

[5] B. Ataie-Ashtiani and G. Shobeyri, "Numerical simulation of landslide impulsive waves by incompressible smoothed particle hydrodynamics," *International Journal for Numerical Methods in Fluids*, vol. 56, no. 2, pp. 209–232, 2010.

[6] H. Ersoy, M. Karahan, K. Gelili, A. Akgün, and B. K. Yahi, "Modelling of the landslide-induced impulse waves in the Artvin Dam reservoir by empirical approach and 3D numerical simulation," *Engineering Geology*, vol. 249, pp. 112–128, 2019.

[7] J. J. Wang, L. L. Xiao, S. N. Ward, and J. Du, "Tsunami squares modeling of the 2007 Dayantang landslide generated waves considering the effects in slide/water interactions," *Engineering Geology*, vol. 284, no. 1-2, article 106032, 2021.

[8] M. Rauter, L. Hoße, R. P. Mulligan, W. A. Take, and F. Løvholt, "Numerical simulation of impulse wave generation by idealized landslides with OpenFOAM," *Coastal Engineering*, vol. 165, article 103815, 2021.

[9] B. Ataie-Ashtiani and A. Nik-khah, "Impulsive waves caused by subaerial landslides," *Environmental Fluid Mechanics*, vol. 8, no. 3, pp. 263–280, 2008.

[10] H. M. Fritz, W. H. Hager, and H. E. Minor, "Landslide generated impulse waves. 2. Hydrodynamic impact craters," *Experiments in Fluids*, vol. 35, no. 6, pp. 520–532, 2003.

[11] V. Heller, W. H. Hager, and H. E. Minor, "Scale effects in subaerial landslide generated impulse waves," *Experiments in Fluids*, vol. 44, no. 5, pp. 691–703, 2008.

[12] B. L. Huang, Y. P. Yin, S. C. Wang et al., "A physical similarity model of an impulsive wave generated by Gongjiafang landslide in Three Gorges Reservoir, China," *Landslides*, vol. 11, no. 3, pp. 513–525, 2014.

[13] J. W. Kamphuis and R. J. Bowering, "Impulse waves generated by landslides," *Coastal Engineering*, vol. 1, pp. 575–588, 1971.

[14] S. B. Yue, M. J. Diao, and L. Wang, "Research on the initial shape and attenuation law of landslide surge," *Journal of Hydraulic Engineering*, vol. 47, no. 6, pp. 816–825, 2016.

[15] B. Ataie-Ashtiani and S. Malek-Mohammadi, "c," *Dam Engineering*, vol. 17, no. 4, pp. 197–222, 2007.

[16] B. L. Huang, Y. P. Yin, and J. M. Tan, "Risk assessment for landslide-induced impulse waves in the Three Gorges Reservoir, China," *Landslides*, vol. 16, no. 3, pp. 585–596, 2019.

[17] Z. G. Tao, Q. Geng, C. Zhu et al., "The mechanical mechanisms of large-scale toppling failure for counter-inclined rock slopes," *Journal of Geophysics and Engineering*, vol. 16, no. 3, pp. 541–558, 2019.

[18] Q. Yin, J. Y. Wu, Z. Jiang et al., "Investigating the effect of water quenching cycles on mechanical behaviors for granites after conventional triaxial compression," *Geomechanics and Geophysics for Geo-Energy and Geo-Resources*, vol. 8, no. 2, pp. 1–28, 2022.

[19] C. Zhu, X. D. Xu, X. T. Wang et al., "Experimental investigation on nonlinear flow anisotropy behavior in fracture media," *Geofluids*, vol. 2019, Article ID 5874849, 9 pages, 2019.

[20] V. Heller, W. H. Hager, and H. E. Minor, *Landslide generated impulse waves in reservoirs-basics and computation*, Editorial Aranzadi, 2009.

[21] H. J. Körner, "Reichweite und geschwindigkeit von bergstürzen und fließschneelawinen," *Rock Mechanics*, vol. 8, no. 4, pp. 225–256, 1976.

[22] B. L. Huang, S. C. Wang, and Y. B. Zhao, "Impulse waves in reservoirs generated by landslides into shallow water," *Coastal Engineering*, vol. 123, pp. 52–61, 2017.

[23] A. Zweifel, D. Zuccala, and D. Gatti, "Comparison between computed and experimentally generated impulse waves," *Journal of Hydraulic Engineering-ASCE*, vol. 133, no. 2, pp. 208–216, 2007.

[24] P. Watts, "Wavemaker curves for tsunamis generated by underwater landslides," *Journal of Waterway Port Coastal and Ocean Engineering*, vol. 124, no. 3, pp. 127–137, 1998.

[25] J. S. Walder, P. Watts, O. E. Sorensen, and K. Janssen, "Water waves generated by subaerial mass flows," *Journal of Geophysical Research: Solid Earth*, vol. 108, no. 5, pp. 2236–2255, 2003.